IBRO Neuroscience Reports 18 (2025) 180–190

Contents lists available at ScienceDirect

IBRO Neuroscience Reports

journal homepage: www.sciencedirect.com/journal/IBRO-Neuroscience-Reports

Research Paper

Multimodal magnetic resonance imaging studies on non-motor symptoms of Parkinson's disease

Weimin Qi [1], Xiaoyan Niu [1], Xiuping Zhan, Yazhou Ren, Jianhang He, Jianxia Li, Xiaolin Hou [*], Haining Li [*]

Neurology Department, General Hospital of Ningxia Medical University, Yinchuan 750004, China

ARTICLE INFO

Keywords:
Parkinson's disease
Multi-modal MRI
Non-motor symptoms
Arterial spin labeling (ASL)
Quantitative susceptibility mapping (QSM)

ABSTRACT

Objective: This study aims to investigate the diagnostic value of multi-modal magnetic resonance imaging (MRI) utilizing arterial spin labeling (ASL), quantitative susceptibility mapping (QSM), and 3D T1-weighted imaging (3DT1WI) in patients with Parkinson's disease (PD). Additionally, it evaluates the relationship between MRI findings and non-motor symptoms associated with PD.

Methods: ASL, QSM, and 3DT1WI scans were performed on 48 PD patients and 46 healthy controls (HC). We extracted and analyzed differences in regional cerebral blood flow (rCBF), magnetic susceptibility, and gray matter density parameters between the two groups. These MRI parameters were correlated with clinical scale scores assessing non-motor symptoms, including cognitive function, sleep quality, olfaction, autonomic function, anxiety, depression, and fatigue. Receiver operating characteristic (ROC) curves were used to evaluate the diagnostic accuracy of each imaging modality in distinguishing PD from HC.

Results: The areas under the ROC curve (AUC) for rCBF, magnetic susceptibility, and gray matter density were 0.941, 0.979, and 0.624, respectively. In PD patients, a negative correlation was found between Unified Parkinson's Disease Rating Scale Part II (UPDRS II) scores and rCBF in the bilateral precuneus. The Pittsburgh Sleep Quality Index (PSQI) scores negatively correlated with rCBF in the left middle temporal gyrus and right middle occipital gyrus. Hamilton Depression Rating Scale (HAMD) scores positively correlated with QSM values in the right supplementary motor area, while scores on the Argentine Smell Identification Test (AHRS) negatively correlated with QSM values in the same area. Disease duration showed a positive correlation with QSM values in the right middle cingulate gyrus. Additionally, PSQI scores positively correlated with QSM values in the left middle cingulate gyrus, and fatigue severity scale (FSS) scores also positively correlated with QSM values in the left middle cingulate gyrus. Gray matter atrophy in the left inferior temporal gyrus was associated with cognitive impairment in PD.

Conclusion: Occipital hypoperfusion and cortical atrophy in the left inferior temporal gyrus may serve as novel imaging biomarkers for PD and are associated with sleep disturbances and cognitive impairment in PD patients. Extensive iron deposition in the bilateral cerebral cortex of PD patients may be a contributing factor to non-motor symptoms such as sleep disturbances and fatigue. Multimodal imaging techniques, including ASL, QSM, and 3DT1WI, can enhance the diagnostic accuracy for PD.

Abbreviations: PD, Parkinson's Diseas; ASL, Arterial Spin Labeling; RCBF, regional Cerebral Blood Flow; UPDRS, Unified Parkinson's Disease Rating Scale; MMSE, Mini Mental State Examination; VBM, VoxelBased Morphometry; 3DT1WI, 3D T1 weighted imaging; HC, healthy controls; H-Y, Modified Hoehn and Yahr Clinical Staging; MRI, Magnetic Resonance Imaging; TIV, total intracranial volume; AHRS, Argentinean Smell Test; SCOPA-AUT, Scales for Outcomes in Parkinson's Disease - Autonomic Dysfunction; PSQI, Pittsburgh Sleep Quality Index; HAMD, Hamilton Depression Rating Scale; HAMA, Hamilton Anxiety Rating Scale; FSS, Fatigue Severity Scale; AUC, area under the curve; PDQ-39, Parkinson's Disease Quality of Life Questionnaire; ROC, Receiver Operating Characteristic; PET, Positron Emission Tomography Scan; RBD, Rapid Eye Movement Sleep Behavior Disorder; DTI, Diffusion Tensor Imaging; DKI, Diffusion Kurtosis Imaging; Rs-fMRI, Resting-State Functional Magnetic Resonance Imaging; NMMRI, Neuromelanin Magnetic Resonance Imaging.

* Corresponding authors.

E-mail addresses: 2324030306@qq.com (W. Qi), nxy1077@163.com (X. Niu), 2684482632@qq.com (X. Zhan), 2653123960@qq.com (Y. Ren), hjh18195126361@163.com (J. He), 2376120086@qq.com (J. Li), 1399581963@163.com (X. Hou), lhnwww@126.com (H. Li).

[1] Weimin Qi and Xiaoyan Niu made equal contributions to this article and are co-first authors.

https://doi.org/10.1016/j.ibneur.2025.01.003
Received 27 July 2024; Accepted 4 January 2025
Available online 6 January 2025

Introduction

Parkinson's disease (PD) is a neurodegenerative disorder characterized by the degeneration and death of dopaminergic neurons in the substantia nigra (Tolosa et al., 2021). Clinically, it is primarily recognized by motor symptoms, including muscle rigidity, resting tremors, bradykinesia, and postural and gait disturbances. Additionally, PD manifests a range of non-motor symptoms, such as cognitive decline, autonomic dysfunction, psychiatric and behavioral abnormalities, and olfactory impairment (Todorova et al., 2014). Notably, these non-motor symptoms often precede motor symptoms, sometimes by several years, and are linked to dopamine deficiency (Schapira and Tolosa, 2010). As the disease advances, non-motor symptoms like cognitive impairment, sleep disturbances, and autonomic dysfunction progressively dominate, severely affecting the patient's quality of life (Chaudhuri et al., 2006). Despite this, the clinical diagnosis of PD still largely depends on its characteristic clinical presentations, as effective biological markers remain lacking (Bae et al., 2021). Furthermore, research on non-motor symptoms has been relatively limited (Salawu et al., 2010). In recent years, with advances in magnetic resonance imaging (MRI) technology, multimodal MRI has emerged as a promising potential biomarker for PD.

Patients with PD exhibit widespread cortical perfusion abnormalities (Pagano et al., 2016). me researchers propose that the degeneration of dopaminergic neurons can alter the brain's microvascular environment, resulting in reduced cerebral perfusion, which in turn contributes to neurodegeneration and decreased brain metabolism (Dayan and Sklerov, 2021). Using dopamine-specific positron emission tomography (PET) to measure regional cortical blood flow in PD patients, significant reductions in perfusion have been observed in the frontal, parietal, temporal, cingulate, and occipital cortices, as well as in the striatum (Jakobson Mo et al., 2022). Although PET and single-photon emission computed tomography are effective tools for monitoring cortical perfusion changes in PD, they are costly, involve radiation exposure, and require lengthy scanning times (Pagano et al., 2016). arterial spin labeling (ASL) imaging offers a non-invasive alternative by labeling water protons in the blood with radiofrequency pulses and generating perfusion maps without the need for contrast agents (Wang and Liu, 2015). ASL also provides higher spatial resolution and faster acquisition times compared to traditional imaging methods. Roberto et al. identified reduced perfusion in specific cerebellar regions of PD patients using ASL imaging (Erro et al., 2020). Lin et al. further demonstrated that both PD and PD with dementia patients exhibit widespread cortical hypoperfusion, with dopaminergic medications improving hypoperfusion in the frontal lobe and cerebellum (Lin et al., 2016). Voxel-based whole--brain analysis using ASL imaging allows for automated comparative assessments of cortical perfusion across the entire brain, reducing the subjective biases associated with manual region-of-interest segmentation. This approach shows great potential as a biomarker for the early diagnosis of PD (Erro et al., 2020; Cheng et al., 2020).

Recent studies have indicated that patients with PD exhibit increased iron deposition within the nigrostriatal pathway. This heightened iron accumulation is thought to be associated with the chelation of neuromelanin in the dopaminergic neurons of the substantia nigra (Brammerloh et al., 2021). The excess iron in this region generates free radicals and interacts with α-synuclein, contributing to one of the mechanisms implicated in PD onset (Sian-Hülsmann et al., 2011). Quantitative susceptibility mapping (QSM) technology leverages phase information to detect local magnetic field variations and derives susceptibility maps through complex deconvolution of the magnetic field, thus enabling precise quantification of tissue iron content (Wang and Liu, 2015). Brain iron deposition in PD patients is believed to be linked to clinical symptoms such as bradykinesia and cognitive decline. Several studies, using QSM imaging, have identified iron accumulation in the substantia nigra as a hallmark of PD (Guan et al., 2017). Additionally, Yuto et al. found that striatal iron deposition in PD patients may be associated with cognitive impairment (Uchida et al., 2020).

Research utilizing structural MRI has demonstrated widespread cortical atrophy in PD patients (Ibarretxe-Bilbao et al., 2009). Volumetric MRI allows for the quantitative analysis of the area, volume, and thickness of atrophied brain regions. However, conventional T1-weighted MRI has limited diagnostic sensitivity for PD and cannot reliably detect subtle cortical volume changes (Ali and Morris, 2015). In contrast, 3D T1-weighted imaging (3DT1WI) provides higher resolution and three-dimensional imaging capabilities, enabling clearer visualization of brain structures in PD patients, with typical scan times under five minutes. Using 3DT1WI for voxel-based morphometry (VBM) analysis, researchers have detected cortical atrophy in PD patients (Chen et al., 2019; Tir et al., 2009), which correlates strongly with cognitive impairment (Pourzinal et al., 2021). Mitsunori et al. found that VBM analysis could effectively differentiate PD from multiple system atrophy (Tsuda et al., 2019), while Tara et al. observed that cortical gray matter atrophy is evident even in the early stages of PD (Madhyastha et al., 2015). VBM analysis based on 3DT1WI has the potential to serve as a rapid and efficient biomarker for the early diagnosis of PD.

In conclusion, this study aims to: 1) Assess the diagnostic utility of multimodal imaging techniques, including QSM, ASL, and 3DT1WI, in PD. 2) Examine the relationship between various MRI metrics from QSM, ASL, and 3DT1WI sequences and non-motor symptoms of PD, such as cognitive impairment, autonomic dysfunction, sleep disturbances, and olfactory deficits. These investigations will deepen the understanding of multimodal MRI applications in diagnosing PD and evaluating non-motor symptoms, ultimately improving diagnostic accuracy for PD.

Materials and methods

Clinical data collection

This study was approved by the Ethics Committee of the General Hospital of Ningxia Medical University, and written informed consent was obtained from all participants. Between June 2021 and June 2023, patients with PD who met the inclusion criteria, along with HC who volunteered to participate, were recruited from the Neurology Outpatient and Inpatient Departments of our hospital. The inclusion criteria were as follows: 1) PD patients were required to meet the clinical diagnostic criteria of the UK Parkinson's Disease Society Brain Bank (Hughes et al., 1992) and have a confirmed diagnosis of idiopathic PD by a neurologist specializing in movement disorders. 2) Participants were excluded if they had a history of cerebrovascular disease, epilepsy, moderate to severe depression, or other neuropsychiatric conditions. 3) All participants had to be able to tolerate MRI, have no contraindications for MRI (e.g., claustrophobia or cardiovascular stents), and provide informed consent. 4) Routine cranial MRI had to show no abnormalities, such as cerebrovascular diseases or severe demyelinating conditions. Ultimately, 48 PD patients and 46 age- and gender-matched healthy controls were included in the study. All PD patients underwent comprehensive assessments, including the UPDRS Part I, II, and III, Mini-Mental State Examination (MMSE), modified Hoehn and Yahr scale (H-Y), Argentine Olfactory Reduction Scale (AHRS), Parkinson's Disease Questionnaire (PDQ-39), Scales for Outcomes in Parkinson's Disease - Autonomic Dysfunction (SCOPA-AUT), Pittsburgh Sleep Quality Index (PSQI), Hamilton Depression Scale (HAMD), Hamilton Anxiety Scale (HAMA), and Fatigue Severity Scale (FSS). Additional data, such as age, gender, disease duration, and other general demographic information, were also collected.

MRI data acquisition and processing

Equipment

All participants underwent imaging using a 3.0T high-performance gradient superconducting MRI scanner (uMR 770) manufactured by Shanghai United Imaging Healthcare Co, Ltd. A 24-channel head coil

was employed for image acquisition, and a soft cushion was used to stabilize the head and minimize motion artifacts. During the scanning process, participants were instructed to keep their eyes closed while remaining awake. For PD patients, medications were administered to ensure they were in the "on" state, reducing the likelihood of head movement and improving image quality.

Scanning sequence parameters

All participants underwent scanning with 3DT1WI, T2-weighted imaging, and T2 fluid-attenuated inversion recovery sequences to rule out other organic brain diseases, followed by QSM and ASL sequences. 3DT1WI: Acquired using a 3D T1 magnetization-prepared rapid gradient echo sequence with the following parameters: field of view = 256 × 230 mm, matrix = 256 × 230, repetition time = 6.94 ms, echo time= 3.0 ms, flip angle = 9°, and slice thickness = 1 mm. ASL: Acquired using a pseudo-continuous arterial spin labeling sequence with these parameters: field of view = 224 × 240 mm, matrix = 150 × 160, repetition time= 5 s, echo time = 14.08 ms, flip angle = 150°, labeling duration = 1500 ms, post-labeling delay = 2001 ms, and slice thickness = 3 mm. QSM: Acquired using a gradient echo sequence with the following parameters: voxel size = 1 × 1 × 1 mm^3, repetition time= 28.3 s, echo time = 3.2 s, number of echoes = 7, flip angle = 15°, and acquisition time = 10 min.

Image preprocessing

ASL preprocessing. rCBF maps for all subjects were generated using the uNity2.0 workstation, with CBF calculated according to the recommended values from the International Society for Magnetic Resonance in Medicine. rCBF was expressed in ml/min/100 g (Hughes et al., 1992). For group-level analysis, rCBF images were spatially normalized using the SPM12 toolbox in Matlab 2021b (MathWorks, MA, USA). The normalization process was as follows: First, 3DT1WI and ASL images were manually reoriented to ensure proper alignment. Next, an affine transformation was applied to map each subject's CBF image onto their reoriented 3DT1WI anatomical image. The 3DT1WI anatomical images were then segmented into gray matter, white matter, and cerebrospinal fluid. During segmentation, modulation was applied to the images to correct for deformation effects on signal intensity. Finally, both the 3DT1WI and CBF images were registered to standard Montreal Neurological Institute space. To enhance the signal-to-noise ratio, the registered CBF images were standardized and spatially smoothed using an 8 mm Gaussian kernel (Erro et al., 2020; Cheng et al., 2020; Liu et al., 2022).

QSM preprocessing. QSM images were obtained using the default processing pipeline on a uNity 2.0 workstation, which included four steps: field map estimation, field map unwrapping, background field removal, and dipole deconvolution. The first step, field map estimation, involves estimating the field map from the magnitude and phase images acquired using a three-dimensional multi-echo gradient echo sequence. The second step, field map unwrapping, involves unwrapping the field map obtained in the first step. The third step, background field removal, removes the background field resulting from both non-ideal homogeneous field and the susceptibility distribution in the background region, leaving only the tissue field generated by the tissue's susceptibility distribution. The fourth step involves dipole deconvolution of the tissue field to solve for the susceptibility distribution (Wang and Liu, 2015; Acosta-Cabronero et al., 2017; Uchida et al., 2019).

Subsequently, QSM and 3DT1WI were manually realigned to ensure accurate co-registration. An affine transformation was applied to map each subject's QSM image onto its realigned 3DT1WI anatomical image. Spatial normalization was performed using the SPM12 toolbox to align the images with a standard template. The DPABI toolbox was used for further normalization of the standardized images to enhance data consistency. The images were smoothed with a 6 mm kernel, and a gray matter mask was applied to exclude cerebrospinal fluid and white matter regions.

3DT1WI preprocessing. The 3DT1WI images for all subjects were acquired using the uNity2.0 workstation and manually corrected to minimize deformation during registration. Segmentation was performed using the SPM12 and Cat12 toolboxes in Matlab 2021, dividing the images into gray matter, white matter, and cerebrospinal fluid. The segmented images were rigidly aligned to the Montreal Neurological Institute space template, and a specific tissue template was generated using the Diffeomorphic Anatomical Registration Through Exponentiated Lie Algebra algorithm for diffeomorphic anatomical registration. Each individual's images were then modulated and normalized to enhance data consistency and comparability. Finally, all images were smoothed with an 8 mm Gaussian kernel (Chen et al., 2019) to improve the signal-to-noise ratio, and a gray matter mask was applied to exclude non-relevant regions.

Statistical analysis

Preprocessed QSM, ASL, and 3DT1WI imaging data will be analyzed using the SPM12 toolbox with voxel-wise multiple comparison correction (Family-Wise Error, cluster sizes >500, $p < 0.001$) (Guillaume and Karl, 2017). Brain regions will be identified using the Anatomical Automatic Labeling template, and variable values from statistically significant regions will be extracted. Statistical analysis will be performed using SPSS version 27.0. Data normality will be assessed using the Shapiro-Wilk test. For normally distributed data with equal variances, independent samples t-tests will be used to compare variables between groups. For data that do not meet the assumption of equal variances, Mann-Whitney U tests will be conducted for non-parametric comparisons. Pearson correlation analysis will be used for normally distributed data, while Spearman correlation analysis will be applied to non-normally distributed data and ordinal variables. A significance level of $p < 0.05$ will be considered statistically significant. Receiver Operating Characteristic (ROC) curve analysis will be used to assess the accuracy of individual sequences (ASL, QSM, 3DT1WI) in distinguishing PD patients from HC. Additionally, binary logistic regression and ROC curve analysis will be used to evaluate the accuracy of pairwise combinations of these sequences for differentiating PD from HC.

Results

Demographic and clinical data of PD and HC groups

There were no significant differences between the PD group and the HC group regarding total intracranial volume (TIV), age, gender, or years of education ($p = 0.391$, 0.079, 0.999, and 0.333, respectively). Detailed demographic and clinical scale data are presented in Table 1.

Correlation of rCBF changes in the PD group with clinical scale scores

Analysis of CBF values between the two groups revealed significant differences in brain perfusion (Fig. 1-A). In the PD group, compared to the healthy controls, CBF values were significantly decreased in several brain regions, including the bilateral occipital lobes, bilateral cuneus, left middle temporal gyrus, left pericalcarine cortex, left angular gyrus, left inferior occipital gyrus, left superior occipital gyrus, left cerebellar vermis, and left precuneus (Fig. 2). In contrast, CBF values were increased in the left cerebellum, right inferior temporal gyrus, right fusiform gyrus, right middle temporal gyrus, right temporal pole, right inferior frontal gyrus, right cingulate gyrus, and right supplementary motor area (Fig. 3).

We also conducted correlation analyses between the CBF values in

Table 1
Demographic and clinical data of the PD and HC groups.

	PD Group	HC Group
Age	59.71 ± 7.40	57.15 ± 6.48
Gentle (female/ male)	25/23	24/22
TIV(cm^3)	1385.50 (1316.50 , 1477.75)	1419.50 (1314.00 , 1486.25)
Course	3.56 (2.17, 5.2)	-
Education (years)	9.22 (5.00, 12.00)	10.50 (7.00, 12.00)
UPDRS I	3.50 (2.40)	-
UPDRS II	9.92 ± 5.33	-
UPDRS III	20.50 (12.33, 29.50)	-
H-Y	1.70 (1.26, 2.27)	-
MMSE	27.58 (24.40,29.35)	29 (27.5, 30)
HAMD	8.00 (3.38 , 13.50)	-
HAMA	9.40 (4.50, 15.57)	-
AHRS	23.10 (20.70, 24.00)	-
SCOPA-AUT	35.77 ± 6.85	-
PSQI	7.00 (4.25, 13.5)	-
FSS	27.00 (17.71 , 42.00)	-
PDQ−39	21.25 (10.25 , 34.00)	-

Demographic and clinical data of the PD and HC groups are presented as mean ± standard deviation or median (25th percentile, 75th percentile).
Abbreviations: TIV = total intracranial volume, UPDRS = Unified Parkinson's Disease Rating Scale, MMSE = Mini-Mental State Examination, H-Y = Hoehn and Yahr clinical staging, AHRS = Argentinean Smell Test, SCOPA-AUT = Scales for Outcomes in Parkinson's Disease - Autonomic Dysfunction, PSQI = Pittsburgh Sleep Quality Index, HAMD = Hamilton Depression Rating Scale, HAMA = Hamilton Anxiety Rating Scale, FSS = Fatigue Severity Scale. PDQ-39 = Parkinson's Disease Quality of Life Questionnaire.

regions showing relative reductions in the PD group and clinical scale scores, including UPDRS I, UPDRS II, UPDRS III, MMSE, and the modified H-Y scale. Notably, UPDRS II scores were negatively correlated with CBF values in the left middle occipital gyrus and bilateral cuneus. Additionally, SCOPA-AUT scores were negatively correlated with CBF values in the bilateral middle occipital gyrus, left calcarine fissure, bilateral cuneus, and left superior occipital gyrus. Moreover, PSQI scores were negatively correlated with CBF values in the left middle temporal gyrus and right middle occipital gyrus (Fig. 4).

Correlation of increased QSM values in the PD group with clinical scale scores

Analysis of QSM imaging revealed significant differences in cortical magnetic susceptibility between the PD and HC groups (Fig. 1-B). Elevated brain iron content was observed in the PD group in regions including the left fusiform gyrus, right supplementary motor area, left precuneus, and the bilateral medial and paracingulate gyri (Fig. 5).

Correlation analysis between QSM values and clinical scale scores revealed several noteworthy findings: Depression scores were positively correlated with QSM values in the right supplementary motor area, while olfactory scale scores were negatively correlated with QSM values in the same region. Additionally, disease duration showed a positive correlation with QSM values in the right middle cingulate gyrus. PSQI scores were positively correlated with QSM values in the left middle cingulate gyrus, as were FSS scores (Fig. 6).

Correlation of reduced gray matter density in the PD group with clinical scale scores

VBM analysis revealed significant differences in cortical gray matter volume between the PD and HC groups (Fig. 1-C). Specifically, PD patients demonstrated reduced gray matter density in the left inferior temporal gyrus compared to healthy controls (Fig. 7). Further correlation analysis showed a positive association between gray matter density in the inferior temporal gyrus and MMSE scores in PD patients, indicating that reduced gray matter in this region may be linked to cognitive decline (Fig. 8).

ROC analysis of MRI metrics

ROC analysis was conducted on the metrics derived from ASL, QSM, and 3DT1WI sequences to evaluate their effectiveness in differentiating between the PD and HC groups. The results showed that both ASL and QSM sequences demonstrated high accuracy in distinguishing PD patients from healthy controls (Fig. 9).

Discussion

This study investigates the clinical applications of multimodal MRI in PD, with a focus on ASL, 3DT1WI, and QSM imaging. Metrics derived from these individual sequences effectively distinguished PD patients from HC, with CBF and QSM showing the highest diagnostic accuracy.

Using ASL-based whole-brain gray matter cortical perfusion measurements, we found that PD patients exhibited reduced CBF in several regions compared to the HC group, including the bilateral middle occipital gyri, bilateral cuneus, left middle temporal gyrus, left pericalcarine cortex, left angular gyrus, left inferior and superior occipital gyri, left cerebellar vermis, and left precuneus. These findings are consistent with previous research that has identified a "posterior brain hypoperfusion" pattern in PD (Kamagata et al., 2011a; Urso et al., 2022; Azamat et al., 2021).

Sleep disturbances are a common non-motor symptom in PD, with

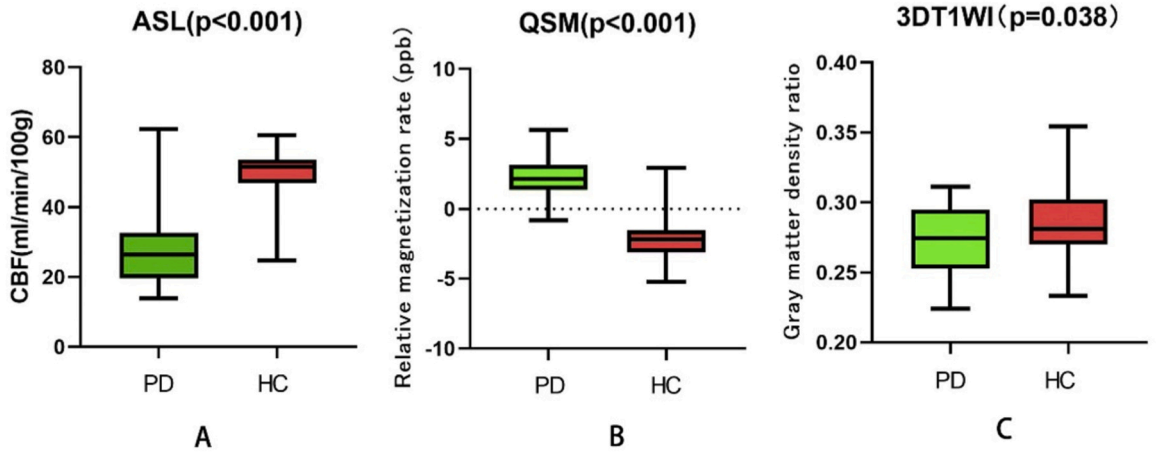

Fig. 1. T-test results of ASL, QSM, and 3D T1WI imaging sequence metrics between the two groups (A = ASL sequence, B = QSM sequence, C = 3DT1WI sequence).

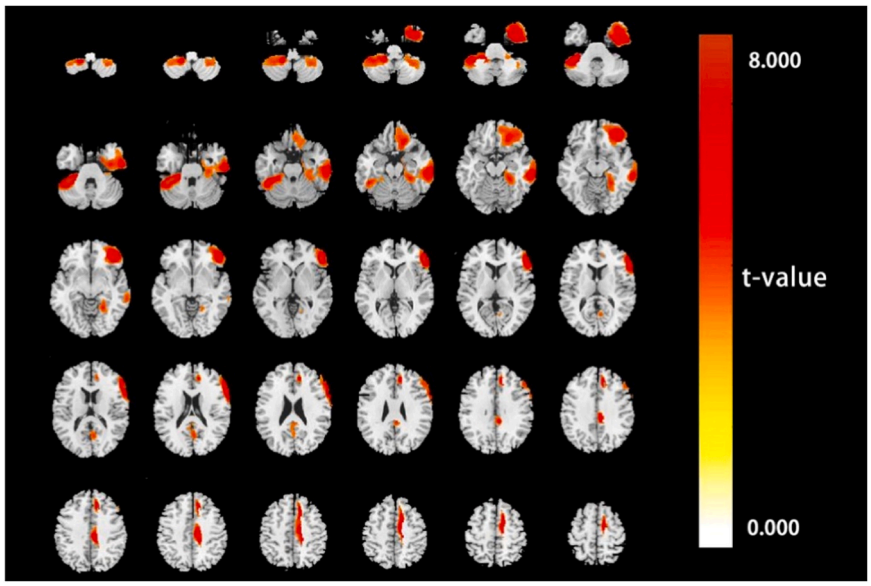

Fig. 2. Distribution map of increased gray matter cortical cerebral blood flow values in the PD group.

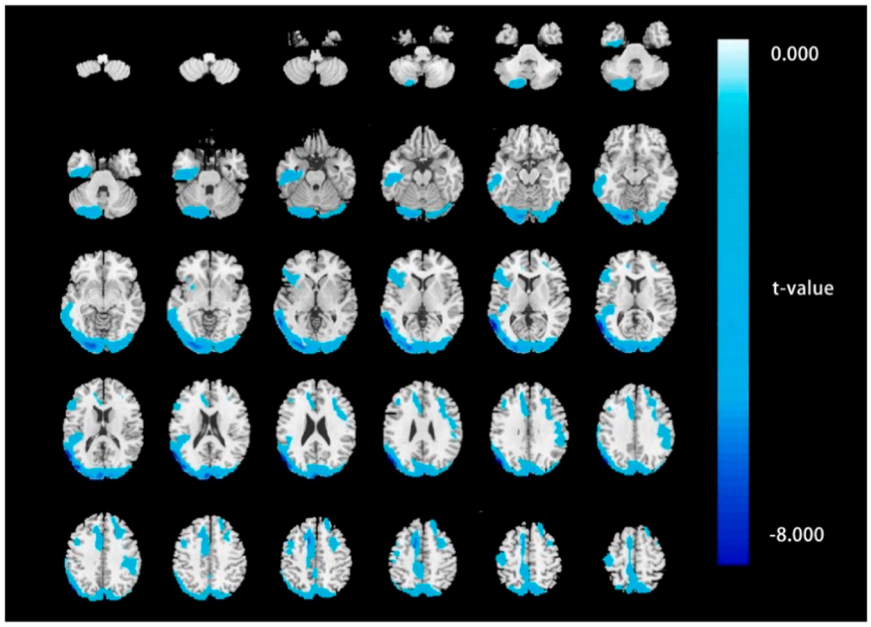

Fig. 3. Distribution map of decreased gray matter cortical cerebral blood flow values in the PD group.

Rapid Eye Movement sleep behavior disorder (RBD)—characterized by nocturnal episodes of shouting—being a notable clinical feature (Postuma et al., 2019). In our study, we found that reduced rCBF in the left middle temporal gyrus and right middle occipital gyrus was associated with poorer sleep quality in PD patients. Ghaderi et al. similarly reported cortical perfusion deficits in regions such as the thalamus, corpus callosum, caudate nucleus, putamen, precuneus, hippocampus, and postcentral gyrus in PD patients with sleep disturbances (Ghaderi et al., 2023).

While the exact mechanisms underlying sleep disturbances and RBD in PD remain unclear, Garcia et al.'s hypothesis of neurodegenerative changes in the midbrain and pons is widely accepted (Valencia Garcia et al., 2018). Additionally, PD patients often experience autonomic dysfunction, characterized by urinary and fecal disturbances, potentially due to α-synuclein pathology spreading from the brain or gut to the autonomic nervous system (Horsager et al., 2020). Our findings suggest that reduced perfusion in the bilateral middle occipital gyrus, left pericalcarine cortex, bilateral cuneus, and left superior occipital gyrus may contribute to autonomic dysfunction in PD. This pattern of reduced posterior cortical perfusion is likely linked to PD-related autonomic dysfunction and supports the previously observed "posterior brain hypoperfusion" characteristic of the disease.

Cognitive impairment is a common non-motor symptom of PD, often emerging in later stages and significantly impacting patients' quality of life. Previous studies have highlighted the critical roles of the frontal and temporal lobes in PD-related cognitive impairment. Additionally, some researchers suggest that reduced occipital cortical perfusion may contribute to cognitive decline in PD (Liu et al., 2022; Kamagata et al., 2011a; Wang et al., 2022). Although the exact mechanism underlying reduced occipital lobe perfusion in PD remains unclear, Kamagata et al. proposed that it may be related to the loss of dopaminergic neurons in the retina (Kamagata et al., 2011b).

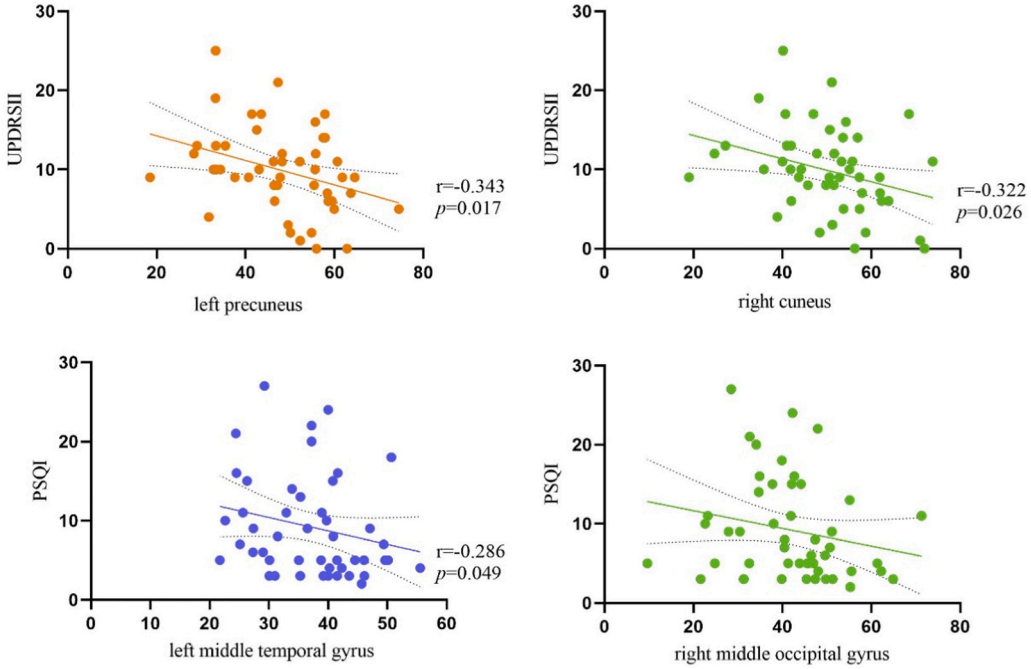

Fig. 4. Correlation analysis results between decreased rCBF regions and clinical scale scores in the PD group (UPDRS = Unified Parkinson's Disease Rating Scale, PSQI = Pittsburgh Sleep Quality Index).

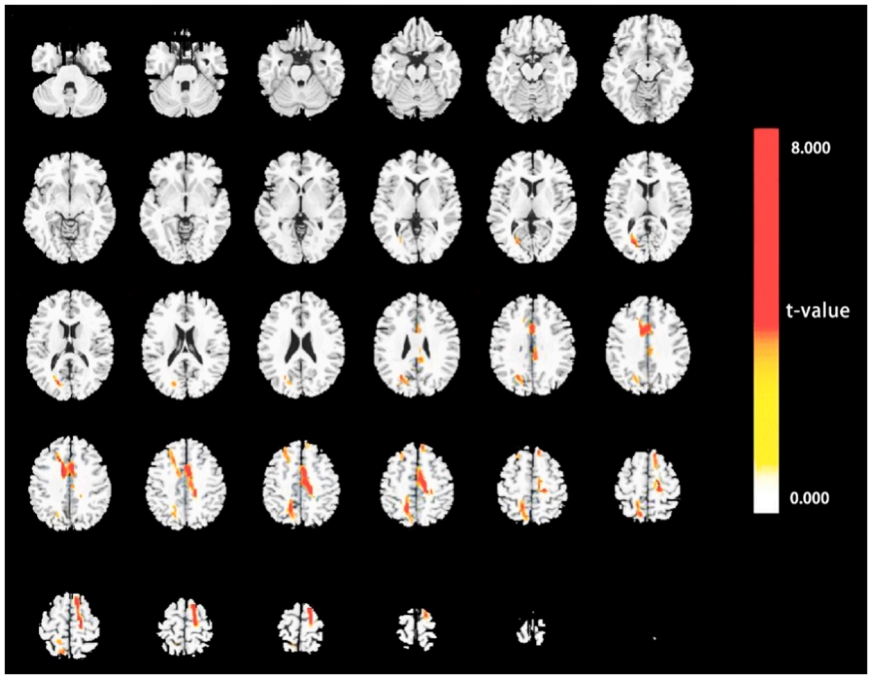

Fig. 5. Distribution map of increased gray matter cortical magnetization in the PD group.

In contrast, we observed increased rCBF in several brain regions of PD patients compared to the HC group, including the left cerebellum, right inferior temporal gyrus, right fusiform gyrus, right middle temporal gyrus, right temporal pole, right inferior frontal gyrus, right cingulate gyrus, and right supplementary motor area. Previous Single Photon Emission Computed Tomography studies have also reported increased perfusion in the putamen, globus pallidus, anterior cerebellum, thalamus, and brainstem in PD patient (Hsu et al., 2007). Similarly, an ASL study by Liu et al. found increased perfusion in the bilateral hippocampus, right cerebellum, and certain subcortical regions in PD patients (Liu et al., 2022).

The exact changes in cortical perfusion in PD are not yet fully understood, making it difficult to identify specific patterns in cortical and cerebellar regions. Some researchers hypothesize that this hyperperfusion may represent a compensatory mechanism in certain brain areas in response to neurodegenerative changes in PD (Liu et al., 2022; Barzgari et al., 2019).

Iron deposition in the brain, which leads to oxidative stress, is a significant factor in the pathogenesis of neurodegenerative diseases like PD (Yan et al., 2023). Compared to NMMRI and R2* imaging, QSM is

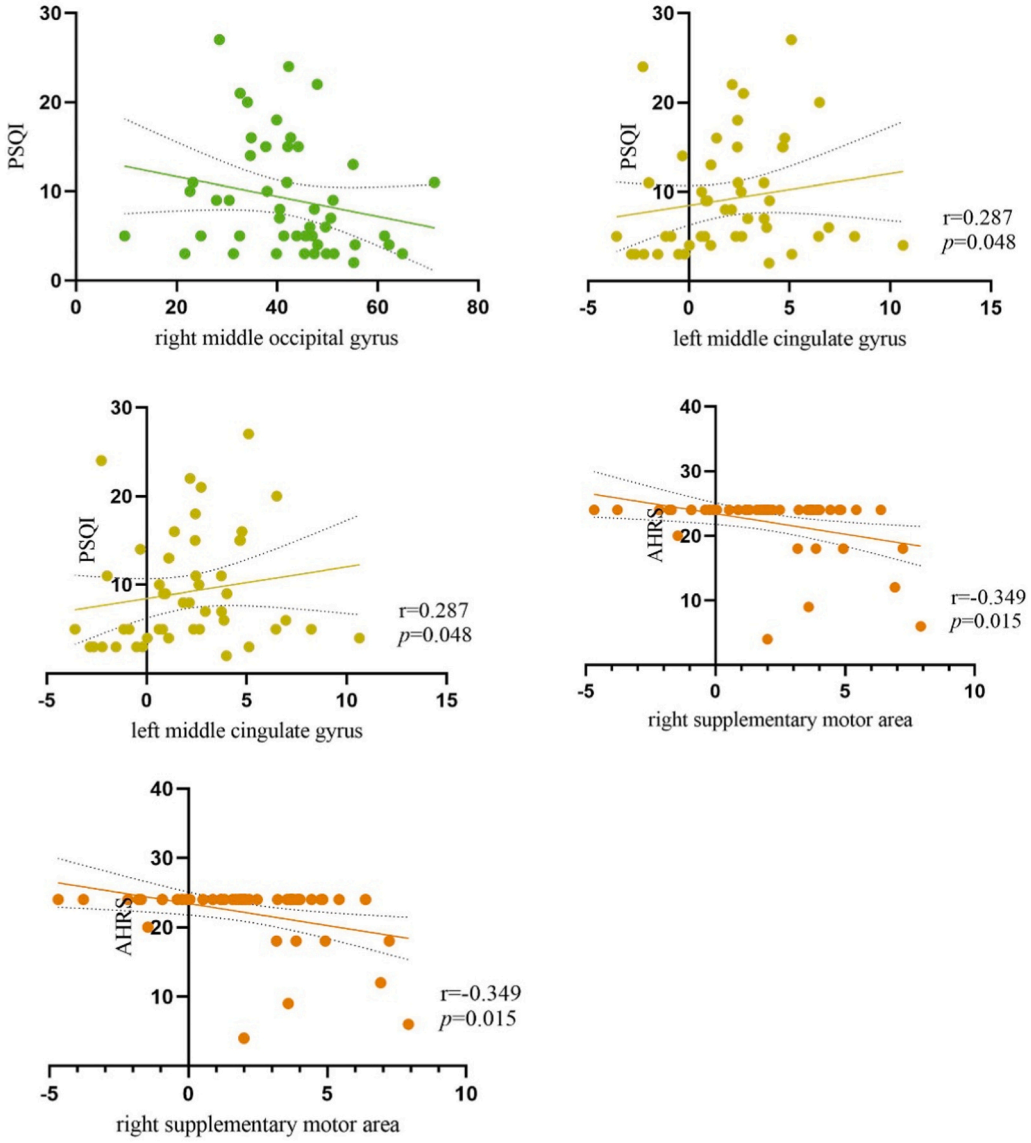

Fig. 6. Correlation analysis results between increased susceptibility regions and clinical scale scores in the PD group (FSS = Fatigue Severity Scale, PSQI = Pittsburgh Sleep Quality Index, AHRS = Argentinean Smell Test).

more sensitive in measuring iron deposition in the dorsolateral substantia nigra (Saikiran, 2020; Takahashi et al., 2018). Previous studies have confirmed increased iron content in the substantia nigra of early PD patients, and this increase in magnetic susceptibility may be related to the loss of neuromelanin in the substantia nigra (Fearnley and Lees, 1991). Pathological studies of human brain tissue have also demonstrated that elevated magnetic susceptibility in the dorsolateral substantia nigra is associated with iron deposition in PD patients (Brammerloh et al., 2021).

PD progression is closely linked to widespread brain dysfunction. However, most prior research has focused on localized brain regions, such as the substantia nigra and red nucleus. Our study primarily investigates changes in brain iron content within the gray matter cortex of PD patients. We found increased iron content in the left fusiform gyrus, right supplementary motor area, left precuneus, and bilateral paracingulate gyri in PD patients. Previous studies have reported heightened magnetic susceptibility in the substantia nigra, red nucleus, right inferior temporal gyrus, right triangular part of the inferior frontal gyrus, left parahippocampal gyrus, and right middle frontal gyrus (Zhao et al., 2022). A voxel-based whole-brain study also revealed increased magnetic susceptibility in the frontal lobe, posterior cingulate gyrus, and insular cortex of PD patients (Thomas et al., 2021). Our findings indicate that increased magnetic susceptibility in PD is predominantly concentrated in the posterior cortical regions, which may be related to decreased metabolic activity in the posterior brain (Alushaj et al., 2023), a result consistent with our ASL imaging findings.

Increased cortical magnetic susceptibility in PD is believed to be associated with disease progression and the worsening of both motor and non-motor symptoms (Guan et al., 2017; Uchida et al., 2019; Song et al., 2021; Tambasco et al., 2019). A study quantifying brain iron content at different stages of PD found that iron accumulation in the red nucleus and substantia nigra increases as the disease progresses (Li et al., 2022). Similarly, our research observed elevated iron content in the right paracingulate gyrus as the disease advanced. Graham et al. reported that increased putamen susceptibility is correlated with PD progression (Song et al., 2021), suggesting that the accumulation of brain iron and subsequent ferroptosis may play a role in PD development (Thomas et al., 2021). These findings highlight QSM as a valuable imaging marker for tracking PD progression and prognosis.

Olfactory dysfunction is an underexplored aspect of PD, yet it can precede motor symptoms by several years. Pathological studies suggest that neuronal loss in structures such as the locus coeruleus and the

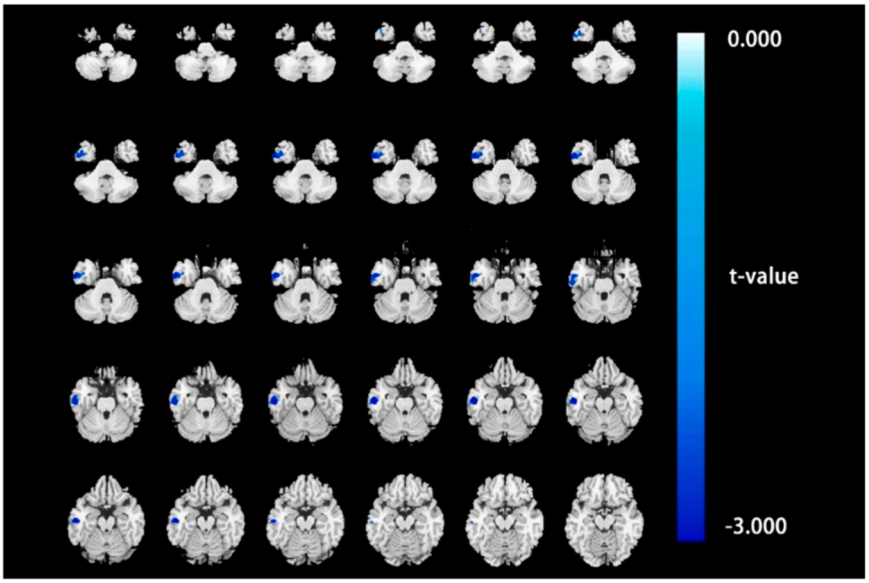

Fig. 7. Distribution map of decreased gray matter cortical density in the PD group.

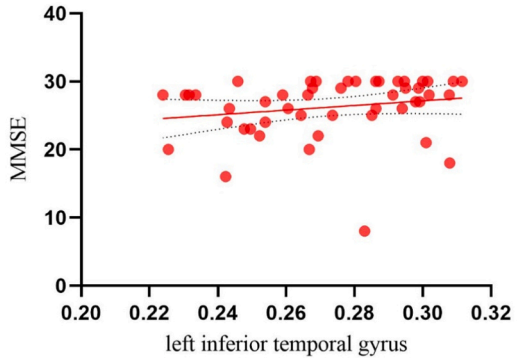

Fig. 8. Correlation analysis results between decreased gray matter density regions and clinical scale scores in the PD group (MMSE = Mini Mental State Examination).

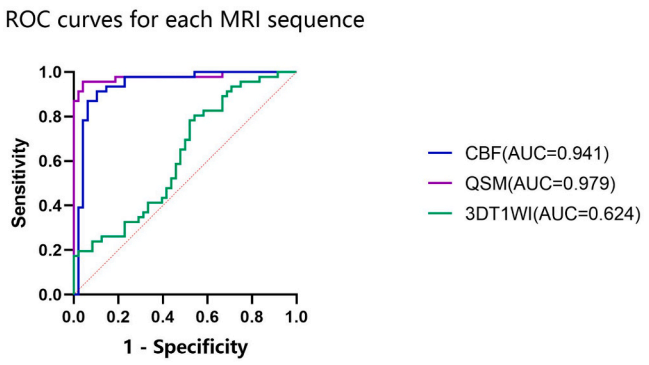

Fig. 9. ROC analysis results for each sequence.

nucleus basalis of Meynert may contribute to olfactory deficits in PD (Doty, 2012). Our correlation analysis using the Argentine Smell Identification Test (ASIT) indicates that the decline in olfactory function in PD patients is associated with increased susceptibility in the right supplementary motor area. Additionally, a susceptibility-based study has confirmed asymmetrical increases in thalamic susceptibility among PD patients with olfactory dysfunction (Hwang et al., 2019). The precise cause of olfactory impairment in PD remains uncertain; however, some researchers hypothesize that dysfunction in the temporal cortex may disrupt the cholinergic basal nucleus, thereby contributing to olfactory decline (Barrett et al., 2021; Leboucq et al., 2013).

Fatigue is another common symptom reported by PD patients, often described as a subjective experience. Our findings demonstrate that increased iron accumulation in the left paracingulate gyrus is correlated with fatigue severity in PD patients, suggesting that fatigue may be associated with structural and functional damage in cortical regions. Furthermore, existing research has linked the severity of fatigue to impairments in the sensorimotor and default mode networks (Tessitore et al., 2016), while Kang et al. have proposed that fatigue in PD patients is connected to damage in white matter tracts (Kang et al., 2020).

Depression is a prevalent non-motor symptom in PD. A study by Liao Haiyan et al. using voxel-mirrored homotopic connectivity analysis found that PD patients with depression show reduced functional connectivity in the bilateral medial frontal gyrus and paracentral lobule (Liao et al., 2020). Additionally, other studies have reported microstructural changes in the prefrontal-temporal regions and associated white matter tracts in depressed PD patients compared to both non-depressed PD patients and healthy controls (Salehi et al., 2022). Our study further identified that increased susceptibility in the right supplementary motor area is associated with higher scores on the HAMD in PD patients, suggesting that iron deposition in this region may be linked to the development of depression in PD.

Dysfunction in specific brain regions can lead to sleep disturbances in PD patients (Ghaderi et al., 2023; Ota et al., 2022). VBM studies have demonstrated that PD patients with sleep disturbances exhibit reduced gray matter volume in the basal ganglia and central precentral-postcentral regions of the left hemisphere (Radziunas et al., 2018). Diffusion tensor imaging (DTI) studies further indicate that PD patients with sleep disturbances display altered fractional anisotropy in the substantia nigra, thalamus, and hypothalamus (Jiang et al., 2022). Our voxel-based whole-brain gray matter cortical susceptibility study suggests that increased susceptibility in the left paracingulate gyrus may contribute to sleep disturbances in PD patients.

Some studies have found that increased iron deposition in the hippocampus and thalamus may contribute to cognitive impairment in PD patients. Visual function impairment may also be associated with increased susceptibility in the frontal, occipital, and parietal cortices (Thomas et al., 2020). A three-year cohort study reported that increased susceptibility in the putamen and right temporal cortex is associated

with cognitive impairment in PD, while increased susceptibility in the red nucleus, substantia nigra, basal ganglia, and insular cortex is linked to the severity of motor impairment (Thomas et al., 2024).

Traditional manual segmentation methods for volumetric image analysis are highly subjective. In contrast, VBM provides an objective and independent spatial segmentation and registration method using high spatial resolution 3DT1WI. Our VBM analysis of 3DT1WI images from both PD and HC groups revealed a potential volume reduction in the left inferior temporal gyrus of PD patients, consistent with Taylor et al.'s findings of unilateral temporal lobe atrophy (Kuhn et al., 2021). A two-year cohort study further confirmed ongoing gray matter volume reduction in the right putamen and right parietal cortex of PD patients, with gray matter density in the midbrain and pons also decreasing as the disease progressed (Fioravanti et al., 2015). Some researchers suggest that this asymmetric cortical volume atrophy may result from insufficient perfusion in specific brain regions of PD patients (Yamaguchi et al., 2022; Pelizzari et al., 2020) contributing to the asymmetric onset and cognitive impairment observed in PD (González-Redondo et al., 2014).

Tinaz et al. reported that early-stage PD patients may exhibit focal cortical thinning in the ventrolateral prefrontal cortex, orbitofrontal cortex, and occipital-parietal regions, with atrophy in these areas potentially linked to emotional disturbances (Tinaz et al., 2011). A retrospective structural MRI study indicated that most PD patients display atrophy in the hippocampus, limbic system, and extensive cortical regions, with those experiencing cognitive impairment showing a more severe pattern of brain atrophy (Ibarretxe-Bilbao et al., 2009). Our study also analyzed the correlation between clinical scales and the volume of the left inferior temporal gyrus in PD patients, revealing a statistically significant association between gray matter density in this region and MMSE scores. This suggests that atrophy in the inferior temporal gyrus may contribute to cognitive impairment in PD patients. Oltra et al. similarly emphasized that reduced gray matter density in the temporal lobe and putamen is a crucial factor in PD-related cognitive impairment (Oltra et al., 2022). Additional research has shown that PD patients with mild cognitive impairment exhibit reduced gray matter volume in the frontal gyrus, precuneus, angular gyrus, temporal lobe, and cerebellum (Donzuso et al., 2021). An independent component analysis and seed-based resting-state functional MRI (rs-fMRI) study reported reduced functional connectivity in the default mode network, involving the anterior cingulate cortex and basal ganglia, in cognitively impaired PD patients (Di Tella et al., 2023). However, some scholars argue that white matter atrophy in PD may be more pronounced and could serve as a more reliable imaging marker for diagnosing cognitive impairment in PD (Güllüoğlu et al., 2023).

For the diagnosis of PD, multimodal MRI imaging is often superior to single-modality imaging. Sana Mohammadi et al. found that increased mean susceptibility and mean kurtosis of the substantia nigra, as assessed by QSM and Diffusion Kurtosis Imaging (DKI) imaging, are characteristic features of PD patients (Mohammadi et al., 2024). MRI sequences based on water diffusion imaging, such as DTI and DKI, in combination with high-resolution imaging, provide a more precise reflection of changes in brain microstructure (Siasios et al., 2016; Wang et al., 2023). Studies have shown that multimodal machine learning models incorporating 3DT1WI, QSM, and DTI outperform single-modality machine learning models in diagnosing PD (Talai et al., 2021). The VBM analysis of 3DT1WI, combined with QSM, has been shown to improve diagnostic accuracy in the early detection of PD as well as progressive supranuclear palsy and multiple system atrophy (Mazzucchi et al., 2022).

This study has several limitations: (Tolosa et al., 2021) The sample size is relatively small and lacks control groups for clinically similar conditions such as essential tremor and multiple system atrophy. Future studies should incorporate larger sample sizes and more diverse control groups to validate the characteristic changes in PD through voxel analysis, brain perfusion, and susceptibility (Todorova et al., 2014). Our study found that regions with decreased rCBF in PD patients are mainly concentrated in the occipital and posterior cortical areas. Future research should further explore visual impairments and other functions associated with these posterior cortical regions in PD patients (Schapira and Tolosa, 2010). As a cross-sectional study, it is challenging to establish a causal relationship between changes in voxel metrics, brain perfusion, and susceptibility with PD progression and clinical manifestations. Longitudinal cohort studies are necessary to confirm these findings.

Conclusion

1. Occipital hypoperfusion and cortical atrophy in the left inferior temporal gyrus may serve as novel imaging biomarkers for PD and are associated with sleep disturbances and cognitive impairment in PD patients.
2. Extensive iron deposition in the bilateral cerebral cortex of PD patients may be a contributing factor to non-motor symptoms such as sleep disturbances and fatigue.
3. Multimodal imaging techniques, including ASL, QSM, and 3DT1WI, can enhance the diagnostic accuracy for PD.

Ethics approval

The study was approved by the Institutional Ethics Committee of General Hospital of Ningxia Medical University, Yinchuan, China. Ethics No: KYLL-2022-0343.

Funding

This article has been supported by the Ningxia Natural Science and Technology Department, under grant number 2022BEG03130. by the Grant from the Key Research and Development Program of Ningxia (No. 2024BEG02011).

Patient's consent

The following line must be mentioned "A full and detailed consent from the patient/guardian has been taken. The patient's identity has been adequately anonymized. If anything related to the patient's identity is shown, adequate consent has been taken from the patient/relative/guardian. The journal will not be responsible for any medico-legal issues arising out of issues related to patient's identity or any other issues arising from the public display of the video".

CRediT authorship contribution statement

Xiaolin Hou: Funding acquisition, Formal analysis, Data curation. **Yazhou Ren:** Data curation, Conceptualization. **Jianhang He:** Conceptualization. **Jianxia Li:** Data curation. **Haining Li:** Investigation, Funding acquisition, Formal analysis, Data curation, Conceptualization. **Xiuping Zhan:** Formal analysis, Data curation, Conceptualization. **Weimin Qi:** Supervision, Software, Resources, Project administration, Methodology, Investigation, Formal analysis, Data curation, Conceptualization. **Xiaoyan Niu:** Investigation, Formal analysis, Data curation, Conceptualization.

Declaration of Generative AI and AI-assisted technologies in the writing process

We did not use AI for writing.

Conflicts of Interest

The author(s) declared no potential conflicts of interest with respect to the research, authorship, and/or publication of this article.

Acknowledgement

The authors gratefully acknowledge the General Hospital of Ningxia Medical University for assistance and support.

References

Acosta-Cabronero, J., Cardenas-Blanco, A., Betts, M.J., Butryn, M., Valdes-Herrera, J.P., Galazky, I., et al., 2017. The whole-brain pattern of magnetic susceptibility perturbations in Parkinson's disease. Brain J. Neurol. 140 (1), 118–131.

Ali, K., Morris, H.R., 2015. Parkinson's disease: chameleons and mimics. Pract. Neurol. 15 (1), 14–25.

Alushaj, E., Hemachandra, D., Kuurstra, A., Menon, R., Ganjavi, H., Sharma, M., et al., 2023. Subregional analysis of striatum iron in Parkinson's disease and rapid eye movement sleep behaviour disorder. NeuroImage Clin. 40, 103519.

Azamat, S., Betul Arslan, D., Erdogdu, E., Kicik, A., Cengiz, S., Eryürek, K., et al., 2021. Detection of visual and frontoparietal network perfusion deficits in Parkinson's disease dementia. Eur. J. Radiol. 144, 109985.

Bae, Y., Kim, J., Sohn, C., Choi, J., Choi, B., Song, Y., et al., 2021. Imaging the substantia nigra in Parkinson disease and other Parkinsonian syndromes. Radiology 300 (2), 260–278.

Barrett, M., Murphy, J., Zhang, J., Blair, J., Flanigan, J., Nawaz, H., et al., 2021. Olfaction, cholinergic basal forebrain degeneration, and cognition in early Parkinson disease. Parkinsonism Relat. Disord. 90, 27–32.

Barzgari, A., Sojkova, J., Maritza Dowling, N., Pozorski, V., Okonkwo, O.C., Starks, E.J., et al., 2019. Arterial spin labeling reveals relationships between resting cerebral perfusion and motor learning in Parkinson's disease. Brain Imaging Behav. 13 (3), 577–587.

Brammerloh, M., Morawski, M., Friedrich, I., Reinert, T., Lange, C., Pelicon, P., et al., 2021. Measuring the iron content of dopaminergic neurons in substantia nigra with MRI relaxometry. NeuroImage 239, 118255.

Chaudhuri, K.R., Healy, D.G., Schapira, A.H., 2006. Non-motor symptoms of Parkinson's disease: diagnosis and management. Lancet Neurol. 5 (3), 235–245.

Chen, Y.S., Chen, H.L., Lu, C.H., Chen, M.H., Chou, K.H., Tsai, N.W., et al., 2019. Reduced lateral occipital gray matter volume is associated with physical frailty and cognitive impairment in Parkinson's disease. Eur. Radiol. 29 (5), 2659–2668.

Cheng, L., Wu, X., Guo, R., Wang, Y., Wang, W., He, P., et al., 2020. Discriminative pattern of reduced cerebral blood flow in Parkinson's disease and Parkinsonism-Plus syndrome: an ASL-MRI study. BMC Med. Imaging 20 (1), 78.

Dayan, E., Sklerov, M., 2021. Autonomic disorders in Parkinson disease: disrupted hypothalamic connectivity as revealed from resting-state functional magnetic resonance imaging. Handb. Clin. Neurol. 182, 211–222.

Di Tella, S., De Marco, M., Baglio, F., Silveri, M.C., Venneri, A., 2023. Resting-state functional connectivity is modulated by cognitive reserve in early Parkinson's disease. Front. Psychol. 14, 1207988.

Donzuso, G., Monastero, R., Cicero, C.E., Luca, A., Mostile, G., Giuliano, L., et al., 2021. Neuroanatomical changes in early Parkinson's disease with mild cognitive impairment: a VBM study; the Parkinson's disease cognitive impairment study (PaCoS). Neurol. Sci. Off. J. Ital. Neurol. Soc. Ital. Soc. Clin. Neurophysiol. 42 (9), 3723–3731.

Doty, R.L., 2012. Olfactory dysfunction in Parkinson disease. Nat. Rev. Neurol. 8 (6), 329–339.

Erro, R., Ponticorvo, S., Manara, R., Barone, P., Picillo, M., Scannapieco, S., et al., 2020. Subcortical atrophy and perfusion patterns in Parkinson disease and multiple system atrophy. Park. Relat. Disord. 72, 49–55.

Fearnley, J.M., Lees, A.J., 1991. Ageing and Parkinson's disease: substantia nigra regional selectivity. Brain J. Neurol. 114 (Pt 5), 2283–2301.

Fioravanti, V., Benuzzi, F., Codeluppi, L., Contardi, S., Cavallieri, F., Nichelli, P., et al., 2015. MRI correlates of Parkinson's disease progression: a voxel based morphometry study. Park. Dis. 2015, 378032.

Ghaderi, S., Karami, A., Ghalyanchi-Langeroudi, A., Abdi, N., Sharif Jalali, S.S., Rezaei, M., et al., 2023. MRI findings in movement disorders and associated sleep disturbances. Am. J. Nucl. Med. Mol. Imaging 13 (3), 77–94.

González-Redondo, R., García-García, D., Clavero, P., Gasca-Salas, C., García-Eulate, R., Zubieta, J.L., et al., 2014. Grey matter hypometabolism and atrophy in Parkinson's disease with cognitive impairment: a two-step process. Brain J. Neurol. 137 (Pt 8), 2356–2367.

Guan, X., Xuan, M., Gu, Q., Xu, X., Huang, P., Wang, N., et al., 2017. Influence of regional iron on the motor impairments of Parkinson's disease: a quantitative susceptibility mapping study. J. Magn. Reson. Imaging JMRI 45 (5), 1335–1342.

Guillaume, F., Friston, K.J., 2017. Analysis of family-wise error rates in statistical parametric mapping using random field theory. Hum. Brain Mapp. 40 (7).

Güllüoğlu, H., Hünerli, D., Çakmur, R., Çolakoğlu, B.D., Ada, E., Yener, G., 2023. Structural and functional changes in mild cognitive impairment in Parkinson's disease. Medicina 60 (1).

Horsager, J., Andersen, K., Knudsen, K., Skjærbæk, C., Fedorova, T., Okkels, N., et al., 2020. Brain-first versus body-first Parkinson's disease: a multimodal imaging case-control study. Brain J. Neurol. 143 (10), 3077–3088.

Hsu, J.L., Jung, T.P., Hsu, C.Y., Hsu, W.C., Chen, Y.K., Duann, J.R., et al., 2007. Regional CBF changes in Parkinson's disease: a correlation with motor dysfunction. Eur. J. Nucl. Med. Mol. Imaging 34 (9), 1458–1466.

Hughes, A.J., Daniel, S.E., Kilford, L., Lees, A.J., 1992. Accuracy of clinical diagnosis of idiopathic Parkinson's disease: a clinico-pathological study of 100 cases. J. Neurol. Neurosurg. Psychiatry 55 (3), 181–184.

Hwang, E.J., Ryu, D.W., Lee, J.E., Park, S.H., Choi, H.S., Kim, J.S., 2019. Magnetic resonance imaging assessment of the substrate for hyposmia in patients with Parkinson's disease. Clin. Radiol. 74 (6), 489.e9-.e15.

Ibarretxe-Bilbao, N., Tolosa, E., Junque, C., Marti, M.J., 2009. MRI and cognitive impairment in Parkinson's disease. Mov. Disord. 24 (2), S748–S753.

Jakobson Mo, S., Axelsson, J., Stiernman, L., Riklund, K., 2022. Validation of dynamic [(18)F]FE-PE2I PET for estimation of relative regional cerebral blood flow: a comparison with [(15)O]H(2)O PET. EJNMMI Res. 12 (1), 72.

Jiang, Y., An, H., Xi, Q., Yang, W., Xie, H., Li, Y., et al., 2022. Diffusion tensor imaging reveals deep brain structure changes in early Parkinson's disease patients with various sleep disorders. Brain Sci. 12 (4).

Kamagata, K., Motoi, Y., Hori, M., Suzuki, M., Nakanishi, A., Shimoji, K., et al., 2011a. Posterior hypoperfusion in Parkinson's disease with and without dementia measured with arterial spin labeling MRI. J. Magn. Reson. Imaging. JMRI 33 (4), 803–807.

Kamagata, K., Motoi, Y., Hori, M., Suzuki, M., Nakanishi, A., Shimoji, K., et al., 2011b. Posterior hypoperfusion in Parkinson's disease with and without dementia measured with arterial spin labeling MRI. J. Magn. Reson. Imaging. JMRI 33 (4), 803–807.

Kang, S., Bang, M., Hong, J., Oh, J., Kim, J., Han, Y., et al., 2020. Neural and dopaminergic correlates of fatigue in Parkinson's disease. J. Neural Transm. 127 (3), 301–309.

Kuhn, T., Becerra, S., Duncan, J., Spivak, N., Dang, B.H., Habelhah, B., et al., 2021. Translating state-of-the-art brain magnetic resonance imaging (MRI) techniques into clinical practice: multimodal MRI differentiates dementia subtypes in a traditional clinical setting. Quant. Imaging Med. Surg. 11 (9), 4056–4073.

Leboucq, N., Menjot de Champfleur, N., Menjot de Champfleur, S., Bonafé, A., 2013. The olfactory system. Diagn. Interv. Imaging 94 (10), 985–991.

Li, K.R., Avecillas-Chasin, J., Nguyen, T.D., Gillen, K.M., Dimov, A., Chang, E., et al., 2022. Quantitative evaluation of brain iron accumulation in different stages of Parkinson's disease. J. Neuroimaging Off. J. Am. Soc. Neuroimaging 32 (2), 363–371.

Liao, H., Fan, J., Shen, Q., Cai, S., Wang, M., Wang, C., et al., 2020. Alterations of interhemispheric functional connectivity in Parkinson's disease with depression: a resting-state functional MRI study. Front. Hum. Neurosci. 14, 193.

Lin, W.C., Chen, P.C., Huang, Y.C., Tsai, N.W., Chen, H.L., Wang, H.C., et al., 2016. Dopaminergic therapy modulates cortical perfusion in parkinson disease with and without dementia according to arterial spin labeled perfusion magnetic resonance imaging. Medicine 95 (5), e2206.

Liu, Z., Zhang, Y., Wang, H., Xu, D., You, H., Zuo, Z., et al., 2022. Altered cerebral perfusion and microstructure in advanced Parkinson's disease and their associations with clinical features. Neurol. Res. 44 (1), 47–56.

Madhyastha, T.M., Askren, M.K., Boord, P., Zhang, J., Leverenz, J.B., Grabowski, T.J., 2015. Cerebral perfusion and cortical thickness indicate cortical involvement in mild Parkinson's disease. Mov. Disord. 30 (14), 1893–1900.

Mazzucchi, S., Del Prete, E., Costagli, M., Frosini, D., Paoli, D., Migaleddu, G., et al., 2022. Morphometric imaging and quantitative susceptibility mapping as complementary tools in the diagnosis of parkinsonisms. Eur. J. Neurol. 29 (10), 2944–2955.

Mohammadi, S., Ghaderi, S., Mohammadi, H., Fatehi, F., 2024. Simultaneous increase of mean susceptibility and mean kurtosis in the substantia nigra as an MRI neuroimaging biomarker for early-stage Parkinson's disease: a systematic review and meta-analysis. J. Magn. Reson. Imaging JMRI.

Oltra, J., Uribe, C., Segura, B., Campabadal, A., Inguanzo, A., Monté-Rubio, G.C., et al., 2022. Brain atrophy pattern in de novo Parkinson's disease with probable RBD associated with cognitive impairment. NPJ Park. Dis. 8 (1), 60.

Ota, Y., Kanel, P., Bohnen, N., 2022. Imaging of sleep disorders in pre-Parkinsonian syndromes. Curr. Opin. Neurol. 35 (4), 443–452.

Pagano, G., Niccolini, F., Politis, M., 2016. Imaging in Parkinson's disease. Clin. Med. 16 (4), 371–375.

Pelizzari, L., Di Tella, S., Rossetto, F., Laganà, M.M., Bergsland, N., Pirastru, A., et al., 2020. Parietal perfusion alterations in Parkinson's disease patients without dementia. Front. Neurol. 11, 562.

Postuma, R., Iranzo, A., Hu, M., Högl, B., Boeve, B., Manni, R., et al., 2019. Risk and predictors of dementia and parkinsonism in idiopathic REM sleep behaviour disorder: a multicentre study. Brain J. Neurol. 142 (3), 744–759.

Pourzinal, D., Yang, J.H.J., Bakker, A., McMahon, K.L., Byrne, G.J., Pontone, G.M., et al., 2021. Hippocampal correlates of episodic memory in Parkinson's disease: a systematic review of magnetic resonance imaging studies. J. Neurosci. Res. 99 (9), 2097–2116.

Radziunas, A., Deltuva, V.P., Tamasauskas, A., Gleizniene, R., Pranckeviciene, A., Petrikonis, K., et al., 2018. Brain MRI morphometric analysis in Parkinson's disease patients with sleep disturbances. BMC Neurol. 18 (1), 88.

Saikiran, P., 2020. Effectiveness of QSM over R2* in assessment of parkinson's disease - a systematic review. Neurol. India 68 (2), 278–281.

Salawu, F.K., Danburam, A., Olokoba, A.B., 2010. Non-motor symptoms of Parkinson's disease: diagnosis and management. Niger. J. Med. J. Natl. Assoc. Resid. Dr. Niger. 19 (2), 126–131.

Salehi, M.A., Mohammadi, S., Gouravani, M., Javidi, A., Dager, S.R., 2022. Brain microstructural alterations of depression in Parkinson's disease: a systematic review of diffusion tensor imaging studies. Hum. Brain Mapp. 43 (18), 5658–5680.

Schapira, A.H., Tolosa, E., 2010. Molecular and clinical prodrome of Parkinson disease: implications for treatment. Nat. Rev. Neurol. 6 (6), 309–317.

Sian-Hülsmann, J., Mandel, S., Youdim, M.B., Riederer, P., 2011. The relevance of iron in the pathogenesis of Parkinson's disease. J. Neurochem. 118 (6), 939–957.

Siasios, I., Kapsalaki, E.Z., Fountas, K.N., Fotiadou, A., Dorsch, A., Vakharia, K., et al., 2016. The role of diffusion tensor imaging and fractional anisotropy in the evaluation of patients. Neurosurg. Focus.

Song, T., Li, J., Mei, S., Jia, X., Yang, H., Ye, Y., et al., 2021. Nigral iron deposition Is associated with levodopa-induced dyskinesia in Parkinson's disease. Front. Neurosci. 15, 647168.
Takahashi, H., Watanabe, Y., Tanaka, H., Mihara, M., Mochizuki, H., Liu, T., et al., 2018. Quantifying changes in nigrosomes using quantitative susceptibility mapping and neuromelanin imaging for the diagnosis of early-stage Parkinson's disease. Br. J. Radiol. 91 (1086), 20180037.
Talai, A.S., Sedlacik, J., Boelmans, K., Forkert, N.D., 2021. Utility of multi-modal MRI for differentiating of Parkinson's disease and progressive supranuclear palsy using machine learning. Front. Neurol. 12, 648548.
Tambasco, N., Paolini Paoletti, F., Chiappiniello, A., Lisetti, V., Nigro, P., Eusebi, P., et al., 2019. T2*-weighted MRI values correlate with motor and cognitive dysfunction in Parkinson's disease. Neurobiol. Aging 80, 91–98.
Tessitore, A., Giordano, A., De Micco, R., Caiazzo, G., Russo, A., Cirillo, M., et al., 2016. Functional connectivity underpinnings of fatigue in "Drug-Naïve" patients with Parkinson's disease. Mov. Disord. 31 (10), 1497–1505.
Thomas, G.E.C., Hannaway, N., Zarkali, A., Shmueli, K., Weil, R.S., 2024. Longitudinal associations of magnetic susceptibility with clinical severity in Parkinson's disease. Mov. Disord.
Thomas, G.E.C., Leyland, L.A., Schrag, A.E., Lees, A.J., Acosta-Cabronero, J., Weil, R.S., 2020. Brain iron deposition is linked with cognitive severity in Parkinson's disease. J. Neurol. Neurosurg. Psychiatry 91 (4), 418–425.
Thomas, G.E.C., Zarkali, A., Ryten, M., Shmueli, K., Gil-Martinez, A.L., Leyland, L.A., et al., 2021. Regional brain iron and gene expression provide insights into neurodegeneration in Parkinson's disease. Brain J. Neurol. 144 (6), 1787–1798.
Tinaz, S., Courtney, M.G., Stern, C.E., 2011. Focal cortical and subcortical atrophy in early Parkinson's disease. Mov. Disord. 26 (3), 436–441.
Tir, M., Delmaire, C., le Thuc, V., Duhamel, A., Destée, A., Pruvo, J.P., et al., 2009. Motor-related circuit dysfunction in MSA-P: usefulness of combined whole-brain imaging analysis. Mov. Disord. 24 (6), 863–870.
Todorova, A., Jenner, P., Ray Chaudhuri, K., 2014. Non-motor Parkinson's: integral to motor Parkinson's, yet often neglected. Pract. Neurol. 14 (5), 310–322.
Tolosa, E., Garrido, A., Scholz, S., Poewe, W., 2021. Challenges in the diagnosis of Parkinson's disease. Lancet Neurol. 20 (5), 385–397.
Tsuda, M., Asano, S., Kato, Y., Murai, K., Miyazaki, M., 2019. Differential diagnosis of multiple system atrophy with predominant parkinsonism and Parkinson's disease using neural networks. J. Neurol. Sci. 401, 19–26.
Uchida, Y., Kan, H., Sakurai, K., Arai, N., Kato, D., Kawashima, S., et al., 2019. Voxel-based quantitative susceptibility mapping in Parkinson's disease with mild cognitive impairment. Mov. Disord. 34 (8), 1164–1173.
Uchida, Y., Kan, H., Sakurai, K., Inui, S., Kobayashi, S., Akagawa, Y., et al., 2020. Magnetic susceptibility associates with dopaminergic deficits and cognition in Parkinson's disease. Mov. Disord. Off. J. Mov. Disord. Soc. 35 (8), 1396–1405.
Urso, D., Gnoni, V., De Blasi, R., Anastasia, A., Aarsland, D., Chaudhuri, K.R., et al., 2022. Neuroimaging biomarkers in a patient with probable psychiatric-onset prodromal dementia with lewy bodies. Neurology.
Valencia Garcia, S., Brischoux, F., Clément, O., Libourel, P., Arthaud, S., Lazarus, M., et al., 2018. Ventromedial medulla inhibitory neuron inactivation induces REM sleep without atonia and REM sleep behavior disorder. Nat. Commun. 9 (1), 504.
Wang, T., Gao, H., Wang, D., Zhang, C., Hu, K., Zhang, H., et al., 2023. Stem cell-derived exosomes in the treatment of melasma and its percutaneous penetration. Lasers Surg. Med. 55 (2), 178–189.
Wang, Y., Liu, T., 2015. Quantitative susceptibility mapping (QSM): decoding MRI data for a tissue magnetic biomarker. Magn. Reson. Med. 73 (1), 82–101.
Wang, J., Zhang, W., Zhou, Y., Jia, J., Li, Y., Liu, K., et al., 2022. Altered prefrontal blood flow related with mild cognitive impairment in Parkinson's Disease: a longitudinal study. Front. Aging Neurosci. 14, 896191.
Yamaguchi, T., Ikawa, M., Enomoto, S., Shirafuji, N., Yamamura, O., Tsujikawa, T., et al., 2022. Arterial spin labeling imaging for the detection of cerebral blood flow asymmetry in patients with corticobasal syndrome. Neuroradiology 64 (9), 1829–1837.
Yan, S., Lu, J., Li, Y., Cho, J., Zhang, S., Zhu, W., et al., 2023. Spatiotemporal patterns of brain iron-oxygen metabolism in patients with Parkinson's disease. Eur. Radiol.
Zhao, Y., Qu, H., Wang, W., Liu, J., Pan, Y., Li, Z., et al., 2022. Assessing mild cognitive impairment in Parkinson's disease by magnetic resonance quantitative susceptibility mapping combined voxel-wise and radiomic analysis. Eur. Neurol. 85 (4), 280–290.